Available online at www.sciencedirect.com
SCIENCE DIRECT®
Polymer 44 (2003) 4341–4354
polymer
www.elsevier.com/locate/polymer

Miscibility and morphology in blends of poly(L-lactic acid) and poly(vinyl acetate-*co*-vinyl alcohol)

Jun Wuk Park, Seung Soon Im*

Department of Fiber and Polymer Engineering, College of Engineering, Hanyang University, 17 Haengdang-dong, Seongdong-gu, Seoul 133-791, South Korea

Received 12 August 2002; received in revised form 14 February 2003; accepted 5 April 2003

Abstract

Poly(vinyl acetate-*co*-vinyl alcohol) copolymers [P(VAc-*co*-VA)] were prepared by acidic hydrolysis of poly(vinyl acetate) (PVAc) at various reaction time, and the degree of hydrolysis was analyzed by ^{13}C nuclear magnetic resonance spectroscopy (NMR). Blends of poly(L-lactic acid) (PLA) and P(VAc-*co*-VA) were prepared by a solvent casting method using chloroform as a co-solvent. The PLA/PVAc blends exhibited a single glass transition over the entire composition range, indicating that the blends were miscible systems. On the contrary, for the blends with even 10% hydrolyzed PVAc copolymer, the phase separation and double glass transition were observed. With increasing neat PVAc contents, the heat of fusion decreased and the melting peaks shifted to lower temperature. The interaction parameter indicated negative values for up to 10% hydrolyzed samples, but positive values at more than 20% hydrolyzed one. Small angle X-ray scattering analysis revealed that the long period and the amorphous layer thickness increased with PVAc composition, suggesting that a considerable amount of PVAc component located in the interlamellar region. Polarized optical microscopy showed that the texture of spherulites became rougher on increasing the PVAc content. In the case of P(VAc-*co*-VA) copolymer, the intensity of polarized light decreased significantly, indicating that P(VAc-*co*-VA) component seemed to be expelled out of the interfibrillar regions. Scanning electron microscopy analysis revealed that the significant phase separation occurred with increasing the degree of hydrolysis. In the case of 70/30 blend of PLA and P(VAc-*co*-VA) with 30 mol% vinyl alcohol, the P(VAc-*co*-VA) copolymer formed the regular domains with a size of about 10 μm.

Keywords: Blends; Miscibility; Morphology

1. Introduction

Poly(L-lactic acid) (PLA) can be utilized for both ecological and biomedical applications. But its brittleness at room temperature is a major defect for many applications. Moreover, the relatively high price of PLA lowers the possibility of their commercialization. In order to modify various properties or to lower the price, many researches on PLA blends with other polymers have been carried out [1–8].

PLA/poly(vinyl acetate) (PVAc) blends have been reported by Gajria et al. [4] in terms of their miscibility, physical properties, degradation and surface tension. The blends showed a miscible phase, and the mechanical properties of the blends exhibited a synergism in the range of 5 to 30% PVAc content. However, the addition of PVAc to PLA led to a dramatic decrease in the degradation rate for enzymatic degradation. On the contrary, PLA/poly(vinyl alcohol) (PVA) blends have been reported that the non-enzymatic and enzymatic hydrolysis of PLA was accelerated by the presence of the hydrophilic PVA, but these blends was immiscible to induce a phase-separated system [9]. On the basis of these previous works, the blend of PLA and poly(vinyl acetate-*co*-vinyl alcohol) [P(VAc-*co*-VA)] is expected to have enhanced mechanical properties as well as a proper degradation rate if the blend forms a miscible phase at the specific vinyl alcohol content. In the case of P(VAc-*co*-VA) blends with other polymers such as poly(*N*,*N*-dimethylacrylamide) [10], poly(4-vinylpyridine) [11] and poly(β-hydroxybutyrate) (PHB) [12], the copolymer composition has been reported to be a major factor to affect their miscibility. Xing et al. have investigated the miscibility and morphology of blends of PHB and P(VAc-*co*-VA) with various copolymer composition in detail [12]. At low vinyl

* Corresponding author. Tel.: +82-2-2290-0495; fax: +82-2-2297-5859.
E-mail address: imss007@hanyang.ac.kr (S.S. Im).

0032-3861/03/$ - see front matter © 2003 Elsevier Science Ltd. All rights reserved.
doi:10.1016/S0032-3861(03)00346-X

alcohol content (9 mol%), the blend formed a miscible phase in molten state within whole composition range. But at higher vinyl alcohol content, the blends were partially miscible or immiscible systems.

Blends of PLA and PVAc [or P(VAc-*co*-VA)] are semicrystalline/amorphous systems. Generally in this system the morphology is known to depend on the extent of segregation of amorphous polymeric diluents. The diluent molecules can locate in interlamellar regions (between lamellar crystals), interfibrillar regions (between the fibrils or lamellar bundles in spherulites) or interspherulitic regions (between the spherulites). The amorphous diluents are often located at multiple sites, leading to coexistence of different types of morphology [13–17]. These multiple location of the amorphous diluents results in multiple T_g-like transitions, although the polymers themselves are miscible at this temperature [15–17].

The segregation of amorphous diluents is brought by the entropic force associated with the tendency to resume random-coiled conformations and the crystallization driving force of crystallizable components in the interlamellar regions [18]. In addition, these two entropic forces compete against the favorable interaction between the polymeric diluent and the amorphous portion of the crystalline polymer in the interlamellar regions. Therefore, the morphology in semicrystalline/amorphous blend is governed by the exclusion of amorphous components out of interlamellar regions and consequently governed by the magnitude of interaction, the interlamellar distance, and the degree of supercooling. Kinetically, the chain diffusivity and the crystallization rate may also be important factors.

In this study, PLA was blended with PVAc and P(VAc-*co*-VA), and the miscibility of these polymers were studied in consideration of the degree of hydrolysis of the copolymers. Additionally, this study was focused on the crystallization, phase behavior and morphology in a semicrystalline/amorphous phase with various composition ratios.

2. Experimental

2.1. Materials and sample preparation

Poly(L-lactic acid) (PLA) was supplied by Korea Institute of Science and Technology with weight average molecular weights of approximately 367,000. Atactic poly(vinyl acetate) (PVAc) was obtained from Sigma-Aldrich, with weight average molecular weights of approximately 167,000. The samples were dried under vacuum at 3 days before using.

Blends of PLA and poly(vinyl acetate-*co*-vinyl alcohol) [P(VAc-*co*-VA)] were prepared by dissolving in chloroform, subsequently drying at room temperature for 2 days and then in vacuum oven at 40 °C for 5 days.

2.2. Preparation of P(VAc-co-VA)

P(VAc-*co*-VA) copolymers were obtained by a hydrolysis of PVAc at 50 °C in acidic medium. PVAc (5 g/dl) was dissolved in a 9/1 (v/v) solution of methanol–water and hydrochloric acid was added to a concentration of 0.2 M in the solution. The degree of hydrolysis was controlled by the reaction time of 5, 10 and 15 h. The products were precipitated in water, followed by dissolution in methanol and reprecipitation in water.

To determine the degree of hydrolysis, ^{13}C NMR measurements were carried out with VXR/Unity 300 spectrometer at 75 MHz in $CDCl_3$. The intensity of the peaks was determined from the integration curves.

2.3. Differential scanning calorimetry

Thermal characteristics of the blends were measured using Perkin–Elmer DSC-7, previously calibrated with indium and zinc. The polymer sample was heated at 190 °C and kept for 5 min to eliminate thermal history, and then was rapidly cooled to 0 °C. The actual measurement was performed during a second heating from 0 to 190 °C at a heating rate of 10 °C/min. For the isothermally crystallized samples, only second scans were performed.

2.4. Polarized optical microscopy

The sample was first melted on a hot stage at 190 °C for 5 min and then rapidly transferred to another hot stage equilibrated at given crystallization temperature. After annealing for given time periods, the spherulite morphology was observed using Nikon polarized light microscope (OPTIPOTO-POL).

To observe the phase separation more clearly, P(VAc-*co*-VA) were coated with platinum on the surface of the samples after etching in methanol/water solution (9/1 v/v) for 5 min. Etched samples were examined under scanning electron microscope (SEM).

2.5. Synchrotron SAXS measurement

Synchrotron small angle X-ray scattering (SAXS) experiments were performed at the SAXS beamline of the Pohang Accelerator laboratory (PAL) in Pohang, Korea [19]. The X-ray wavelength used was 0.154 nm and the beam size at the focal point is less than 1 mm^2, focused by a platinum-coated silicon premirror through double crystal monochromator. The scattering intensity was detected with a one-dimensional Si diode-array detector with 2048 channels, and the distance between the heating chamber and the detector was about 1.6 m for SAXS. The scattering angle was calculated using a Bragg spacing of 65.3 nm of a chicken tendon collagen as a reference peak for SAXS. The blend samples were heated at a temperature above the melting point of PLA (190 °C) and quickly moved into

Table 1
Assignment of methylene carbon spectra of P(VAc-*co*-VA)

Peaks	Chemical shift (ppm)
$P_{(OH)(OH)}$	45.0
$P_{(OH)(Ac)}$	42.9
$P_{(Ac)(Ac)}$	39.2

Table 2
The degree of hydrolysis of P(VAc-*co*-VA)

Sample name	Hydrolysis time (h)	The degree of hydrolysis (%)
P(Vac-*co*-VA)10	5	11.7
P(Vac-*co*-VA)20	10	20.7
P(VAc-*co*-VA)30	15	31.4

the heating chamber at the desired crystallization temperature. Isothermal crystallization measurements were carried out for 40 min and the scattering profiles were monitored with exposure times of 10 s.

3. Results and discussion

3.1. ^{13}C NMR analysis

In the ^{13}C NMR spectra of PVAc and P(VAc-*co*-VA), the most interesting region is known to that of the methylene region (38–46 ppm) [20–22]. The three well-defined peaks of the methylene region have been assigned to the three dyad sequences (OH, OH), (OH, Ac), (Ac, Ac) as denoted in Table 1. The mole fractions of the dyad sequence can be calculated from the integrated intensities of the three peaks. The vinyl alcohol content (OH) for the copolymers can be derived as following equation:

$$(OH) = (OH, OH) + \frac{(OH, Ac)}{2} \quad (1)$$

The block character of the copolymers is obtained by the expression:

$$\eta = \frac{(OH, Ac)}{2(OH)(Ac)} \quad (2)$$

where η is a measure of deviation from the random character [23]. It takes $0 \leq \eta < 1$ for the block distribution; $\eta = 0$ for block copolymers; $\eta = 1$ for completely random distributions; and $1 < \eta \leq 2$ for alternate-like structures.

Fig. 1 showed the ^{13}C NMR spectra of the methylene region of P(VAc-*co*-VA) on the hydrolysis time. For neat PVAc, only one peak was observed at 39.2 ppm corresponding to (Ac, Ac). The peak of (OH, Ac) dyads was observed at 43 ppm and the peak area increased proportionally with the hydrolysis time. However, the peak at about 45 ppm, which is corresponding to (OH, OH) dyad, did not appear even for the reaction time of 15 h, suggesting that the copolymer had a completely random distribution. The η values calculated by Eq. (2) were higher than unity. We could confirm that the acid hydrolysis was an adequate method for obtaining a random distribution. The vinyl

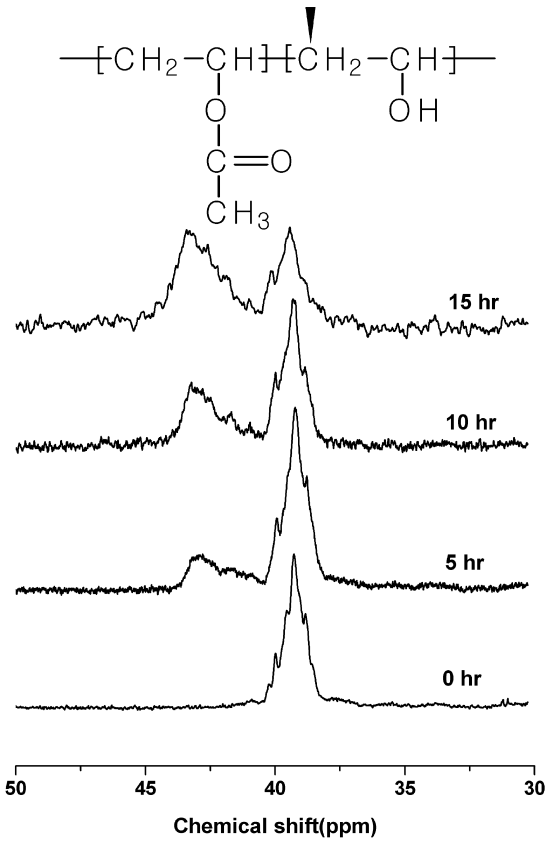

Fig. 1. ^{13}C NMR spectra of the methylene region for P(VAc-*co*-VA).

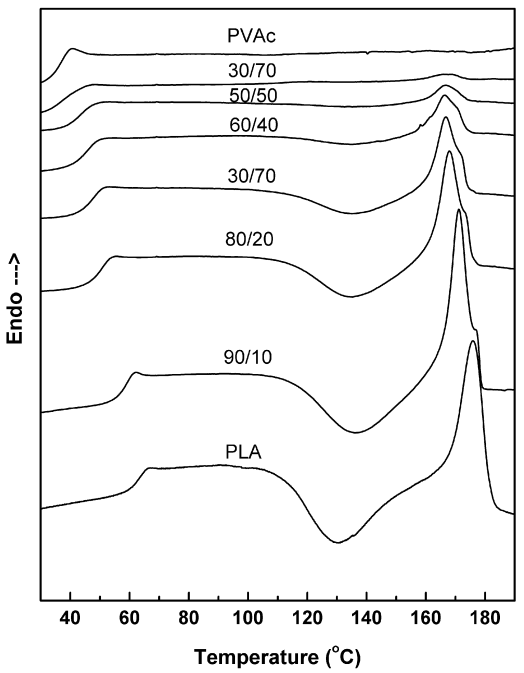

Fig. 2. DSC thermograms of PLA/PVAc blends.

Table 3
Thermal characteristics of PLA/PVAc blends

Mixing ratios of PLA/PVAc	T_g (°C)	T_m (°C)	ΔH_f (J/g)
100/0	62.8	176.1	27.1
90/10	58.1	171.0	26.3
80/20	49.4	168.0	19.0
70/30	46.5	166.7	14.3
60/40	44.9	166.4	9.0
50/50	42.9	166.6	4.8
30/70	38.9	166.0	–
0/100	35.3	–	–

alcohol content for the copolymers was calculated by Eq. (1) and was shown in Table 2. It increased proportionally with the hydrolysis time. For the hydrolysis time of 15 h, the content of vinyl alcohol was about 30%. We used the copolymer hydrolyzed up to 30% because higher hydrolyzed samples were not dissolved in chloroform as a co-solvent for blending with PLA.

3.2. Differential scanning calorimetry

Fig. 2 presented the DSC thermograms of PLA/PVAc blends and their characteristic values were denoted in Table 3. A single glass transition was observed for all the blends compositions. In particular, T_g of the blends is dependent on the blend composition, which indicated the PLA/PVA system to be miscible in the entire composition range. In general, the blend miscibility is often quantified by analyzing its dependence on composition. Traditionally, equations based on the free volume hypothesis have been used to model the composition dependence of the glass transition temperature. They are expressed as the Fox [24] and the Gordon–Taylor equation [25]. The Fox equation is as follows:

$$\frac{1}{T_g} = \frac{W_1}{T_{g1}} + \frac{W_2}{T_{g2}} \tag{3}$$

where W_i is the weight fraction of component i, T_g is the blend T_g and T_{gi} is the glass temperature of neat component i. This equation assumes that the specific heats of the two components are identical. The Gordon–Taylor equation is:

$$T_g = \frac{W_1 T_{g1} + kW_2 T_{g2}}{W_1 + kW_2} \tag{4}$$

where the G–T parameter k is formally equal to $\Delta\alpha_2/\Delta\alpha_1$, and $\Delta\alpha$ is the difference in the thermal expansion coefficient between the liquid and glassy states at T_{gi}. Generally, k is often used as a fitting parameter. In Fig. 3, the solid line showed the calculated curve by the Fox equation and the dot line represented the best fit curve by the Gordon–Taylor equation, which was obtained with a value of $k = 2.8$. Gajria et al. [4] have been reported that the T_g curve with various blend compositions was in good agreement with values calculated by the Fox equation. However, in our work, the observed values were consistent with those calculated by the Gordon–Taylor equation using a value of $k = 2.8$ rather than those by the Fox equation.

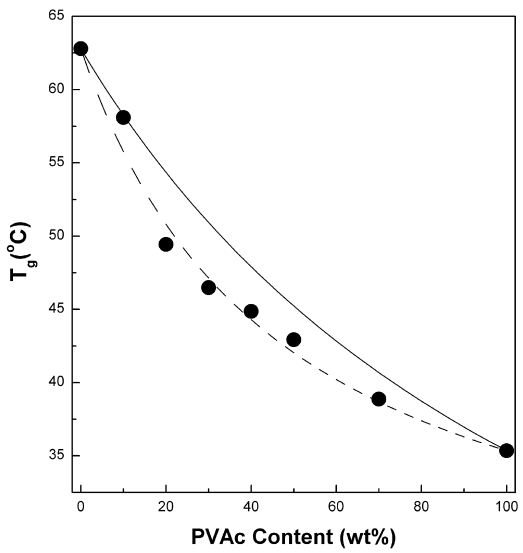

Fig. 3. Variables of the glass transition temperature with blend composition.

When the PVAc content increased, the melting point of PLA was considerably lowered and the heat of fusion decreased. Generally, in miscible blends, the melting point of the crystalline component and the crystallization rate decreased in comparison with pure polymer as a result from favorable thermodynamic interactions at crystal fronts.

Fig. 4 presented the DSC thermograms of the blends of PLA and P(VAc-*co*-VA). In the case of the PLA/P(VAc-*co*-VA)10 blend (Fig. 4(a)), a single glass transition was observed at 90/10 composition. But when the P(VAc-*co*-VA)10 content was more than 10%, double T_g were clearly observed, suggesting that PLA and P(VAc-*co*-VA)10 were immiscible at these compositions. The melting point of the PLA component decreased slightly due to favorable interactions of the P(VAc-*co*-VA)10 component.

For the PLA blends with P(VAc-*co*-VA)20 (Fig. 4(b)), double T_g were observed in the entire composition range, indicating that the 20% hydrolyzed PVAc copolymer was immiscible with PLA in all the compositions. In the case of PLA/P(VAc-*co*-VA)30 blends in Fig. 4(c), the glass transitions looked just like a single transition at 90/10 and 30/70 compositions. But these results seemed to be due to a decrease in the difference of the T_gs between PLA and P(VAc-*co*-VA)30, in fact, the T_g for P(VAc-*co*-VA)30 increased as an extent of about 20 degree compared with neat PVAc by introducing vinyl alcohol group. We thought that the PLA/P(VAc-*co*-VA)30 blends was also immiscible in all the compositions. In conclusion, introduction of vinyl alcohol groups into PVAc lead to immiscible blends with PLA.

Flory–Huggins interaction parameter (χ) is known as

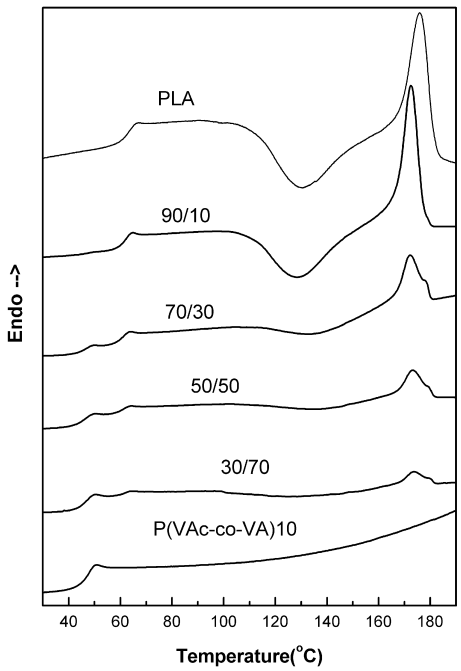

(a)

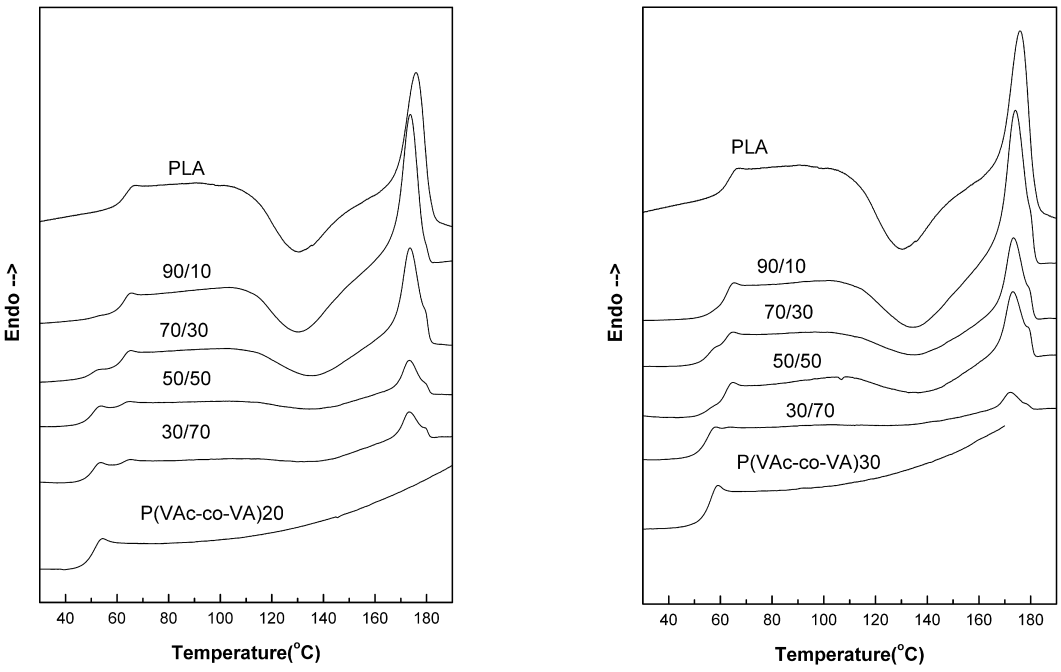

(b) (c)

Fig. 4. DSC thermograms of (a) PLA/P(VAc-*co*-VA)10 blends, (b) PLA/P(VAc-*co*-VA)20 blends, (c) PLA/P(VAc-*co*-VA)30 blends.

another method for estimating the polymer blend miscibility. Melting point depression is one of the most widely used techniques for measure χ because of its simplicity. This approach is based on the assumption that the melting point depression is caused by the thermodynamics mixing of the miscible polymer. Two different methods are often employed to obtain the equilibrium melting point T_m^0. The first is the Gibbs–Thompson approach [26] in which the T_m^0 is obtained from the intercept of a plot of the reciprocal of lamellar thickness versus T_m. The more popular approach is the Hoffman–Weeks extrapolation [27] in which T_m^0 is derived from a plot of T_m versus T_c. In order to apply Flory–Huggins theory [28] to our blend systems, the isothermal crystallization was carried out at the temperature range of 120–160 °C.

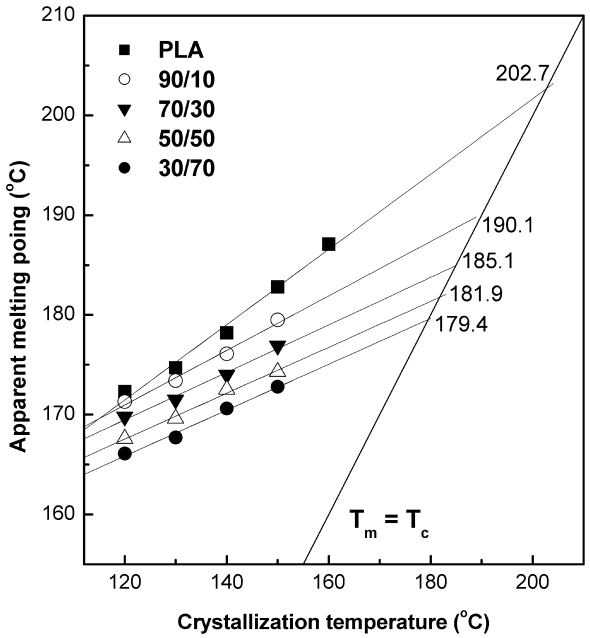

(a)

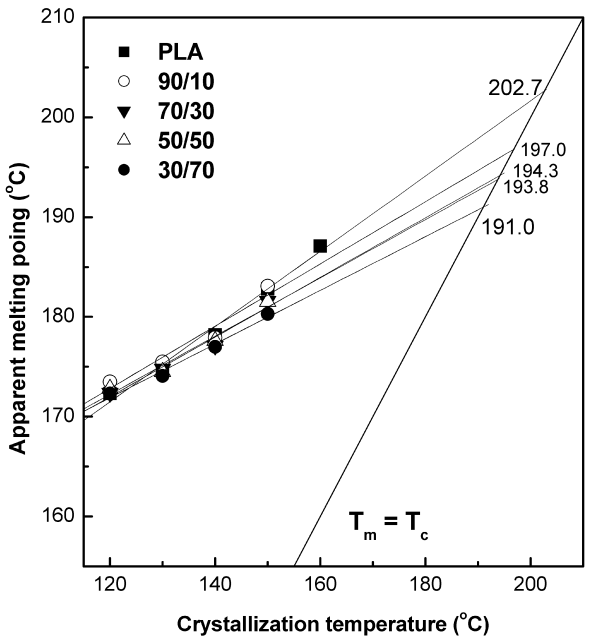

(b)

Fig. 5. Hoffman–Weeks plots for PLA in its blends with (a) PVAc, (b) P(Vac-*co*-VA)10 at various compositions.

Fig. 5(a) showed the Hoffman–Weeks plots for PLA and its blends with PVAc at various compositions. The equilibrium melting point T_m^0 was obtained from the intersection of this line with the $T_m = T_c$ equation. T_m^0 for neat PLA was about 203 °C, which was slightly lower than previously reported values in the range from 207 to 212 °C [29]. In the blends, the equilibrium melting point decreased largely in the early stage but this depression was decreased

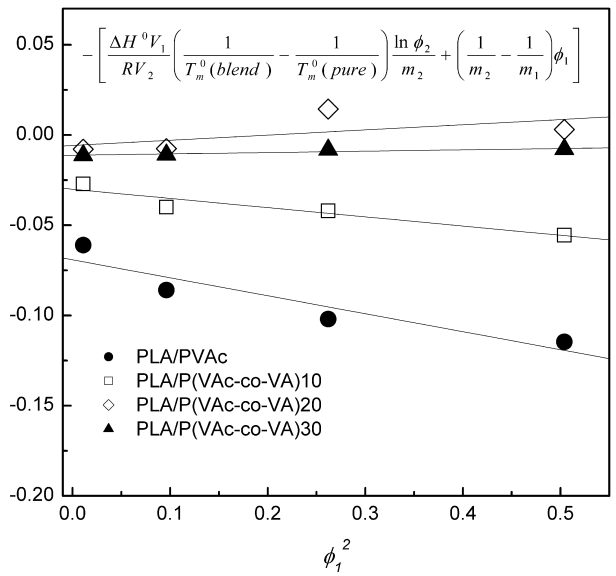

Fig. 6. Plots according to Flory–Huggins equation for PLA/P(VAc-*co*-VA) blends at various compositions.

with increasing PBS content. The maximum extent of this melting point depression was about 23 degree in the 30/70 blends, where T_m^0 was 179.4 °C. In the case of PLA/P(VAc-*co*-VA)10 blends as shown in Fig. 5(b), the melting point depression was smaller than that of PLA/PVA blends. At the 30/70 compositions, the extent of the depression was about 13 degree. For the blends with copolymers containing higher vinyl alcohol content, the melting point depression was not observed. We could obtain the Flory–Huggins interaction parameters with the T_m^0 of the blends.

According to the Flory–Huggins theory, the melting point depression of crystallizable component in compatible blend with non-crystallizable component can be written as follows.

$$\frac{1}{T^0_{m(blend)}} - \frac{1}{T^0_{m(pure)}} = -\frac{RV_2}{\Delta H^0 V_1}\left[\frac{\ln \phi_2}{m_2} + \left(\frac{1}{m_2} - \frac{1}{m_1}\right)\phi_1 + \chi_{12}\phi_1^2\right] \quad (5)$$

Where ΔH^0 is the heat of fusion of the crystalline component, V is the molar volume of the repeat unit, and m and ϕ are the degree of polymerization and volume fraction, respectively. In order to determine the interaction parameter χ_{12}, Eq. (5) can be rewritten as follows.

$$-\left[\frac{\Delta H^0 V_1}{RV_2}\left(\frac{1}{T^0_{m(blend)}} - \frac{1}{T^0_{m(pure)}}\right)\frac{\ln \phi_2}{m_2} + \left(\frac{1}{m_2} - \frac{1}{m_1}\right)\phi_1\right] = \chi_{12}\phi_1^2 \quad (6)$$

Subscripts 1 and 2 refer to the non-crystalline (PVAc or P(VAc-*co*-VA)) and crystalline(PLA) polymers, respectively. If the interaction parameter is independent of blend composition, a plot of the left-hand side versus ϕ_1^2 in Eq. (6) should

Table 4
Interaction parameters of PLA/P(VAc-*co*-VA) blends

Sample name	χ_{12}
PLA/PVAc	−0.10
PLA/P(VAc-*co*-VA)10	−0.04
PLA/P(VAc-*co*-VA)20	0.029
PLA/P(VAc-*co*-VA)30	0.007

give a straight line, of which the slope is equal to χ_{12}. The values of the left-hand side of Eq. (6) from the experimental melting points were calculated using the following parameter values: $\Delta H^0 = 120$ J/cm^3 [30], $m_1 = 1942$, $m_2 = 5097$, $V_1 = 72.3$ cm^3/mol, and $V_2 = 57.14$ cm^3/mol. The volume fractions were calculated from weight fraction using the densities of PLA and PVAc.

Fig. 6 presented the plots of Eq. (6) using the experimental melting temperature of PLA component in PLA/P(VAc-*co*-VA) blends. The interaction parameters could be obtained from a slop of linear fitting line (solid line) and were represented in Table 4.

In the case of PLA/PVAc blend, the linear fitting line had some deviation from actual values, which implied that χ was not independent of the blend composition. In addition, the intercept at $\phi_1^2 = 0$ was not a negligible value, indicating that the depression of the melting point was influenced not only by the interaction between two polymers but also by the morphological effect such as smaller lamellar thickness. But its slope was a certainly

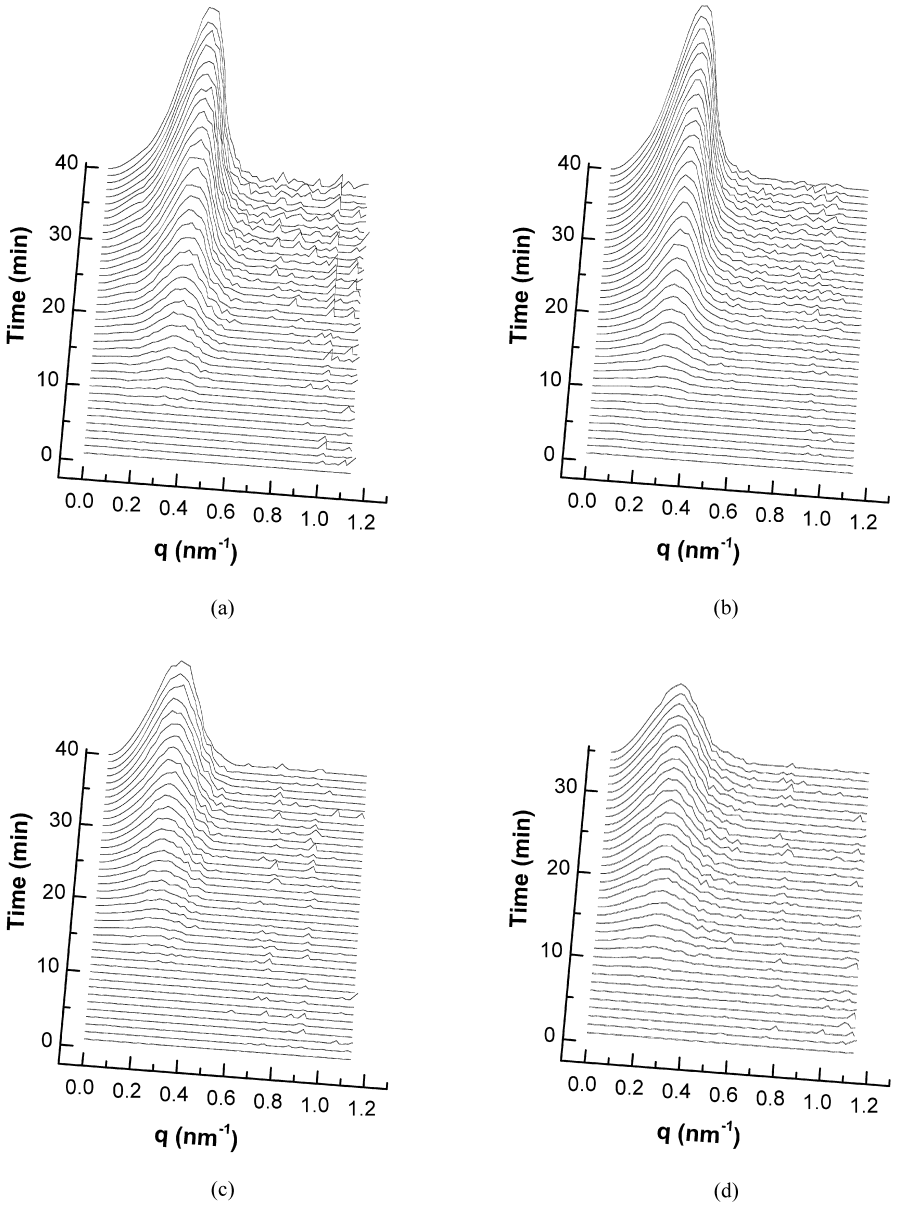

Fig. 7. Evolution of Lorentz-corrected SAXS profiles of (a) neat PLA, (b) PLA/PVAc 90/10, (c) PLA/PVAc 70/30, (d) PLA/PVAc 50/50 isothermally crystallized at 120 °C.

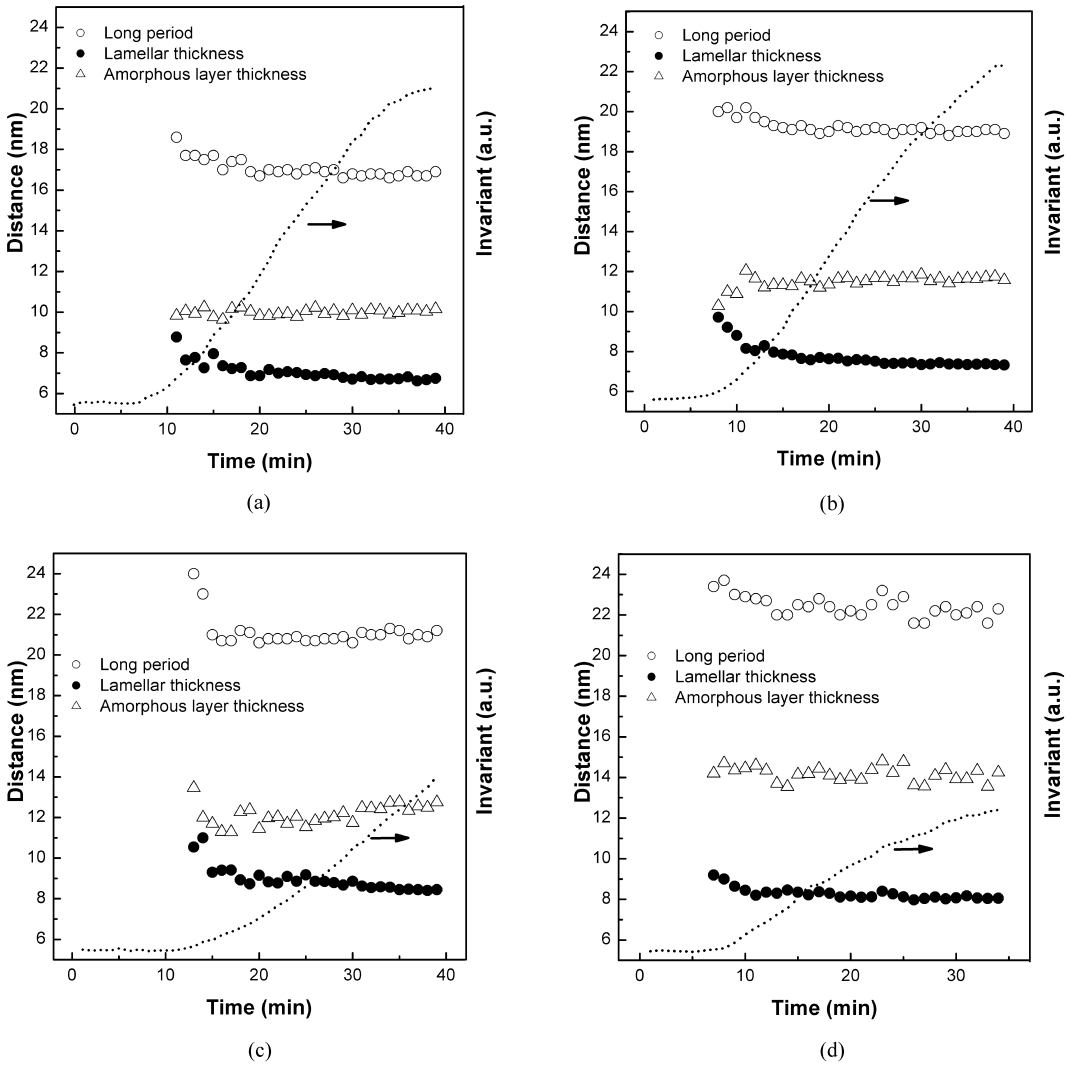

Fig. 8. Morphological variables of (a) neat PLA, (b) PLA/PVAc 90/10, (c) PLA/PVAc 70/30, (d) PLA/PVAc 50/50 isothermally crystallized at 120 °C. The scattering invariant (Q), long period (L), lamellar thickness (l_c) and amorphous layer thickness (l_a) were obtained from the correlation function.

negative value of −0.10. This indicated that the PLA/PVAc polymer blends were thermodynamically miscible, which was consistent with the DSC results showing single T_g in all the composition range.

PLA/P(VAc-*co*-VA)10 blends also exhibited a negative value. But the value was near zero and the melting point depression plot shown in Fig. 6 indicated a non-linear behavior and had a non-zero y-intercept. Therefore, considering DSC results showing double T_g at more than 10% of the P(VAc-*co*-VA)10 content, PLA/PVAc polymer blends seemed to be partially miscible, which was dependent on the composition. For the blends with copolymers containing higher vinyl alcohol content, the interaction parameters showed positive values, suggesting that the blends are thermodynamically immiscible. These blend systems could be expected to show a phase separation behavior in the molten state.

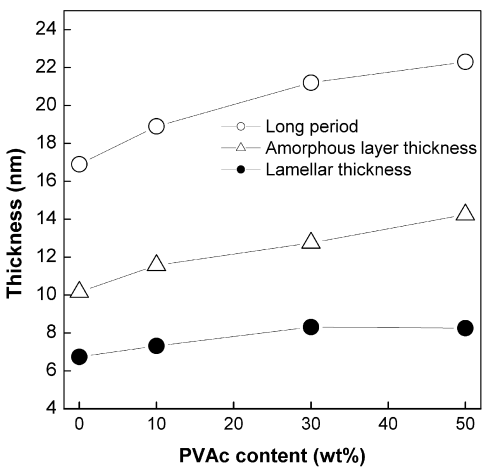

Fig. 9. Plot of morphological parameters as a function of PVAc content for PLA/PVAc blends isothermally crystallized at 120 °C for 35 min.

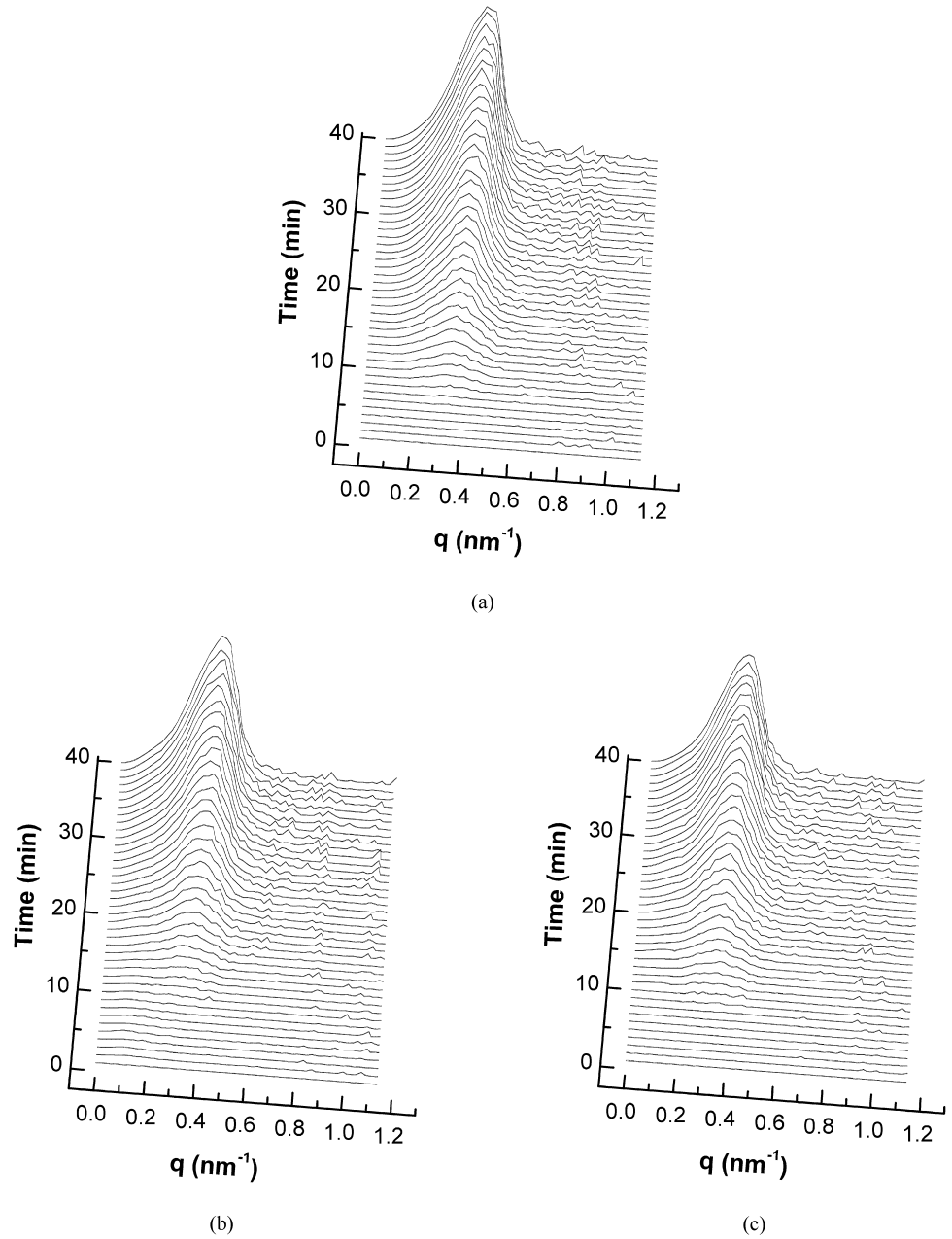

Fig. 10. Evolution of Lorentz-corrected SAXS profiles of (a) PLA/P(VAc-*co*-VA)10 70/30, (b) PLA/P(VAc-*co*-VA)20 70/30, (c) PLA/P(VAc-*co*-VA)30 70/30, isothermally crystallized at 120 °C.

3.3. Synchrotron small angle X-ray scattering analysis

All the synchrotron SAXS data were corrected by the background including a dark current and an empty beam scattering, and were plotted as a smoothed Lorentz-corrected form, Iq^2 vs q, where $q = 4\pi/\lambda \sin(\theta/2)$ (θ = scattering angle, λ = wavelength). Fig. 7 displayed the evolutions of Lorentz-corrected scattering profiles for PLA/PVAc blends during isothermal crystallization at 120 °C for 40 min. For the neat PLA (Fig. 7(a)), a scattering peak around $q = 0.2–0.5\ \mathrm{nm}^{-1}$ started to appear after 10 min and the intensity increased gradually and the peak position shifted gradually to larger scattering vectors (q) with time. The scattering profiles of the PLA/PVAc blends showed similar behavior to that of neat PLA. However, the overall peak intensity decreases and the peak positions shifted slightly to lower q with increasing the PVAc composition.

To discuss the crystallization kinetics, the invariant Q, which is convenient to employ the integrated scattering intensity, was calculated as follows:

$$Q = \int_0^\infty q^2 I(q) \mathrm{d}q \tag{7}$$

In addition, to investigate morphological changes during the isothermal crystallization in more detail, the morphological

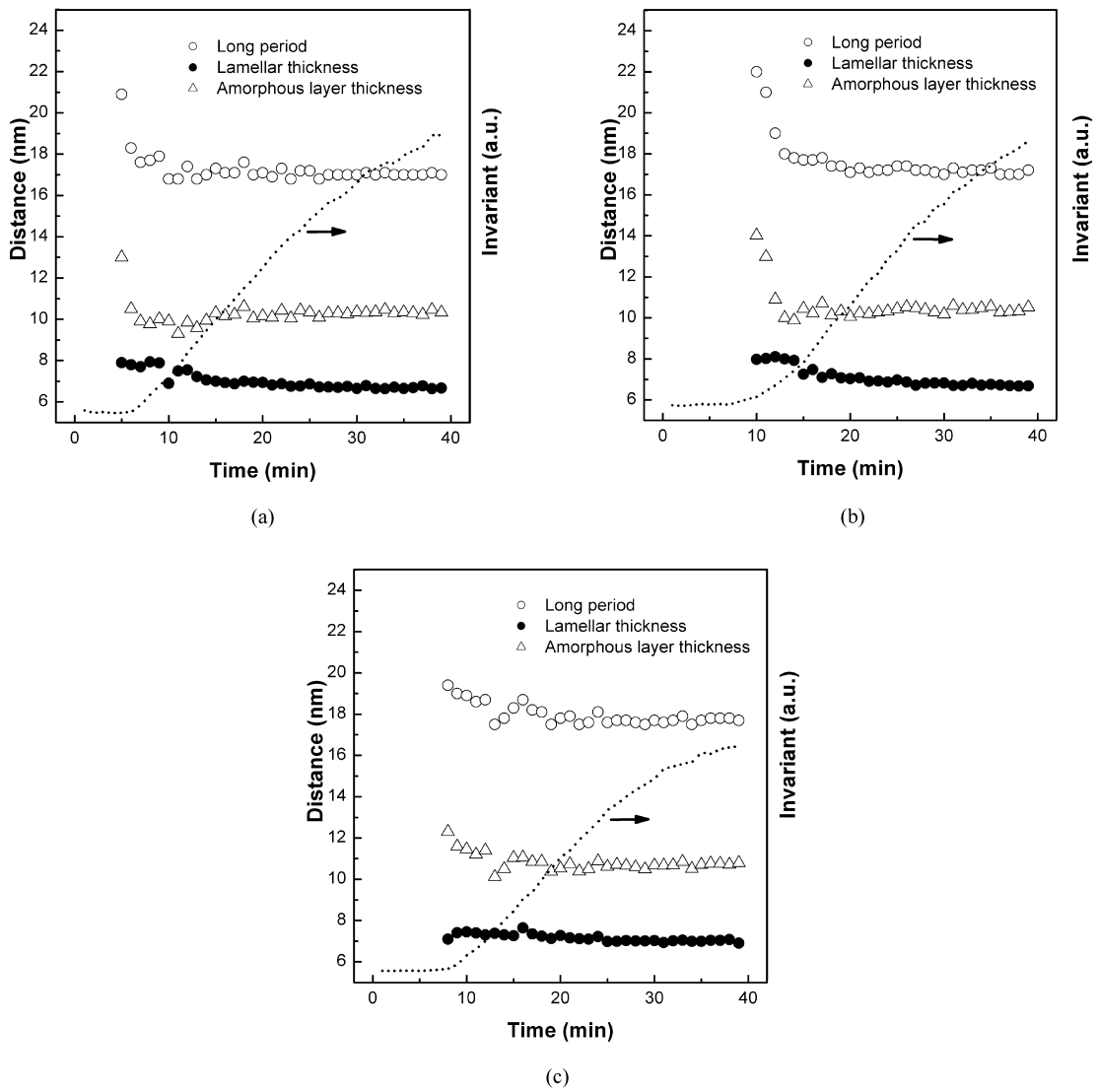

Fig. 11. Morphological variables of (a) PLA/P(VAc-*co*-VA)10 70/30, (b) PLA/P(VAc-*co*-VA)20 70/30, (c) PLA/P(VAc-*co*-VA)30 70/30, isothermally crystallized at 120 °C. The scattering invariant (Q), long period (L), lamellar thickness (l_c) and amorphous layer thickness (l_a) were obtained from the correlation function.

parameters including the long period, the average lamellar thickness and the amorphous-phase thickness were calculated from the normalized one-dimensional correlation function ($\gamma(r)$) evaluated from the scattered intensity $I(q)$ by the following equation [31]:

$$\gamma(r) = \left(\frac{1}{2\pi}\right)^2 \int q^2 I(q)\cos(qr)\mathrm{d}q \tag{8}$$

where r is the correlation distance.

As the experimentally accessible q range was finite, it was necessary to extend the data to both lower and higher q values. The intensity versus q data were linearly extrapolated from the smallest measured q value to zero. Large q values were damped to infinite q by using the Porod law (q^{-4} decay) [32]. The average long period (L) was determined by first maximum in the correlation function, and the average lamellar thickness (l_c) was determined from x-axis values of an intersection point between tangent-line at $\gamma(r) = 0$ and tangent-line at first minimum in the correlation curve. The amorphous phase thickness (l_a) could be calculated with L and l_c ($l_a = L - l_c$).

Fig. 8 presented the morphological parameters for PLA/PVAc blends obtained from the correlation function. For neat PLA (Fig. 8(a)), the scattering invariant exhibited a sigmoidal increase with time, and the long period and the lamellar thickness displayed the high values at the early stage of crystallization and then rapidly decreased as crystallization proceeded. Other researchers have already reported this morphological behavior at the initial crystallization stages [33,34]. The scattering at the beginning of crystallization would be attributed to the thermal fluctuation leading to the electron density difference, which reflected to a high long period on the SAXS profile. As the isothermal

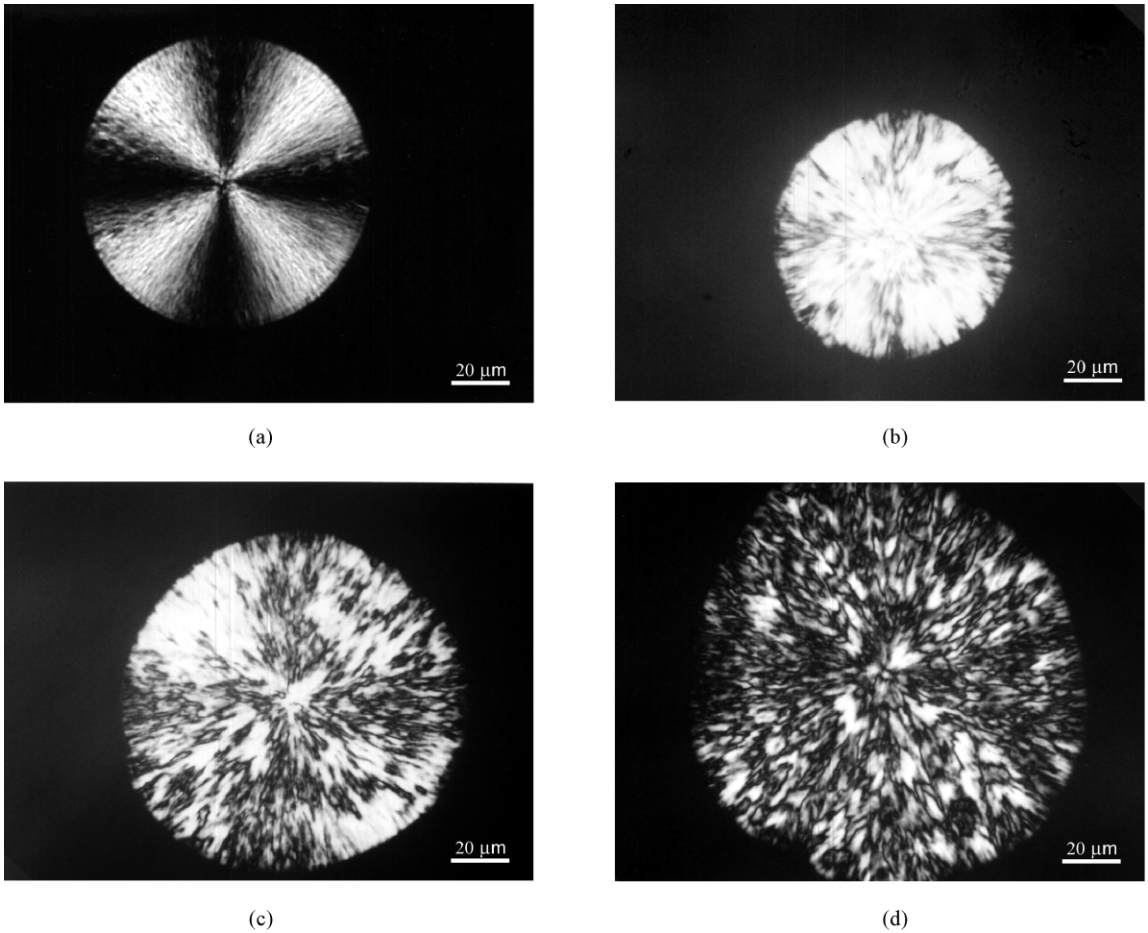

Fig. 12. Polarized optical micrographs of PLA/PVAc blends, isothermally crystallized at 130 °C for various time; (a) neat PLA for 30 min, (b) 70/30 for 50 min, (c) 50/50 for 70 min, (d) 30/70 for 90 min.

crystallization proceeded, the progressive addition of subsidiary thin lamellae along the dominant ones would result in a progressive decrease of the long period and the average lamellar thickness.

In the case of PLA/PBAc blends, the increased rate of the invariant with time became slower and the invariant at 40 min decreased with the PVAc composition, indicating that amorphous PVAc would lower the crystallization rate due to the favorable thermodynamic interaction at the crystal fronts. In addition, the morphological parameters including the long period, the average lamellar thickness and the amorphous layer thickness increased with increasing the PVAc content. The effect of PVAc composition on the morphological parameters for $t = 35$ min was demonstrated in Fig. 9. The amorphous layer thickness increased up to 41% at 50 wt% PVAc content, meaning that most PVAc components located in the interlamellar regions after the PLA component crystallized.

The lamellar thickness also increased from 6.7 to 8.3 nm with the PVAc content. An increase in lamellar thickness by blending has been reported for systems such as poly(ethylene oxide) (PEO)/ethylene–methacrylic acid copolymer (EMAA55), PEO/styrene-*p*-hydroxystyrene copolymer (SHSS50) [35], poly(vinylidene fluofide) (PVF2)/poly(1,4-butylene adipate) (PBA) [36] and polycaprolactone (PCL)/poly(vinylphenol) (PVPh) [37]. The lamellar thickening by blending has been explained by the depression of equilibrium melting point, which was particularly effective in systems involving strong interactions [37].

Fig. 10 showed the evolutions of Lorentz-corrected scattering profiles for PLA/P(VAc-*co*-VA) 70/30 blends during the isothermal crystallization at 120 °C for 40 min, and the variation of the morphological parameters obtained from the correlation function were presented in Fig. 11. The morphological parameters for all the blends exhibited the similar values to those of neat PLA. This result suggests that hydrolyzed P(VAc-*co*-VA) did not affect the crystallization behavior of PLA. As mentioned earlier, T_g observation or melting point depression methods indicated that these blend systems were immiscible in this composition, so that a phase separation between PLA and P(VAc-*co*-VA) seemed to occur first from the molten state. So, we thought that the PLA crystallization seemed to occur selectively in the PLA-rich phase.

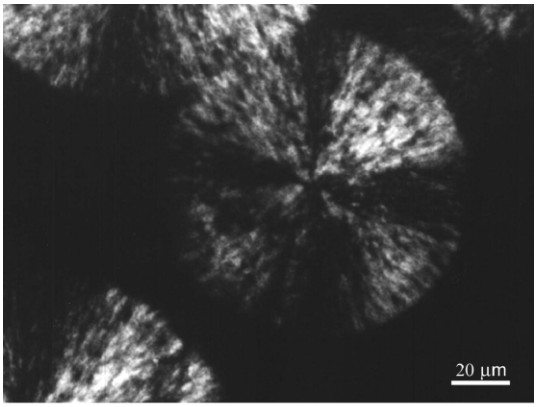

(a)

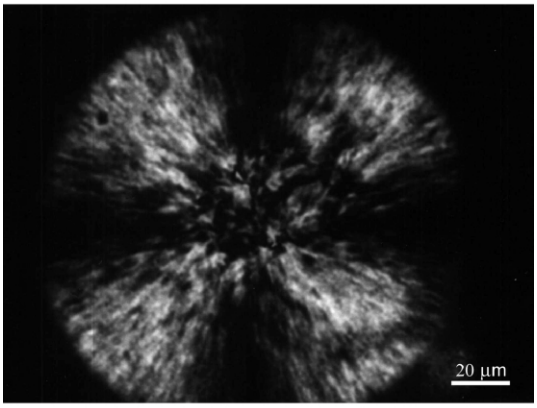

(b)

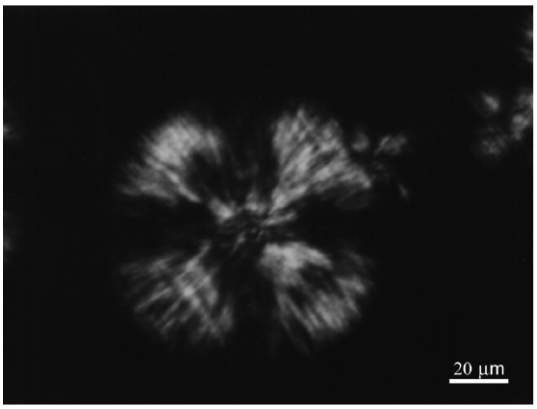

(c)

Fig. 13. Polarized optical micrographs of (a) PLA/P(VAc-*co*-VA)10 70/30, (b) PLA/P(VAc-*co*-VA)20 70/30, (c) PLA/P(VAc-*co*-VA)30 70/30, isothermally crystallized at 130 °C for 30 min.

3.4. Morphology of the blends

Fig. 12 presented the polarized optical micrographs of PLA/PVAc blends at various compositions, after crystallization at 130 °C for 30–90 min. The spherulites of neat PLA showed the familiar Maltese cross birefringence and a good fibril structure grown radially. With increasing PVAc content in the blends, the texture of PLA spherulites become coarser and Maltese cross was disrupted. This texture seemed to be similar to the coarse grained structure of neat PLA crystallized at higher temperature than 150 °C [38]. This might be brought by the low undercooling in the blends due to a decrease in equilibrium melting point. In miscible blends, the banding morphology or opened structure has often been reported as an evidence of the interfibrillar segregation of amorphous diluents [39–41]. In the case of PLA blend, Ohkoshi et al. [39] have been reported the banding texture in the PLA/atactic PHB 75/25 blends, which was not apparent in the spherulite of neat PLA, and suggested that the addition of atactic PHB induced the periodic torsion of growing PLA lamellae. In the PLA/PVAc blends, this banding and opened morphology were not observed. In addition, the long-term crystallization led to the volume filling spherulites even for 30/70 blends, indicating that the interspherulitic segregation did not occur. So, we thought that PVAc components dominantly located in the interlamellar regions, which were consistent with SAXS results as discussed above.

On the contrary, in the PLA/P(VAc-*co*-VA) blends the texture of spherulite became rougher and the overall brightness of polarized light significantly decreased with increasing the vinyl alcohol content in the P(VAc-*co*-VA) component, as shown in Fig. 13. Additionally, the boundary of the spherulite looked open and unclear. In particular, the spherulites did not fill the volume completely at more than 30% P(VAc-*co*-VA) content, even after the isothermal crystallization for 24 h. These results suggested that the P(VAc-*co*-VA) component located dominantly into the interfibrillar regions and was expelled out of PLA spherulites with increasing the P(VAc-*co*-VA) content, as PLA and P(VAc-*co*-VA) were not miscible with each other.

Fig. 14 showed the SEM photographs of PLA/P(VAc-*co*-VA) 70/30 blends extracted by methanol/water solution (9/1 v/v) for 5 min. The methanol/water solution is a good solvent for neat PVAc and P(VAc-*co*-VA) but a poor one for PLA; thus we could selectively remove neat PVAc or P(VAc-*co*-VA) components from the blends and observe the remaining morphology. PLA/PVAc blends displayed smooth surfaces, indicating that the blend formed a homogeneous mixture. But in the case of PLA/P(VAc-*co*-VA) blends, we could observe voids which were placed by P(VAc-*co*-VA) domains extracted by methanol/water solution, and the domain size became larger with increasing the vinyl alcohol content in P(VAc-*co*-VA) component. That is, the phase separation became more significant with the vinyl alcohol content. For 30% vinyl alcohol content, a large number of P(VAc-*co*-VA) domains were regularly distributed with a size of about 10 μm.

4. Conclusions

PLA was blended with PVAc and P(VAc-*co*-VA) and the miscibility, the crystallization behavior and morphology

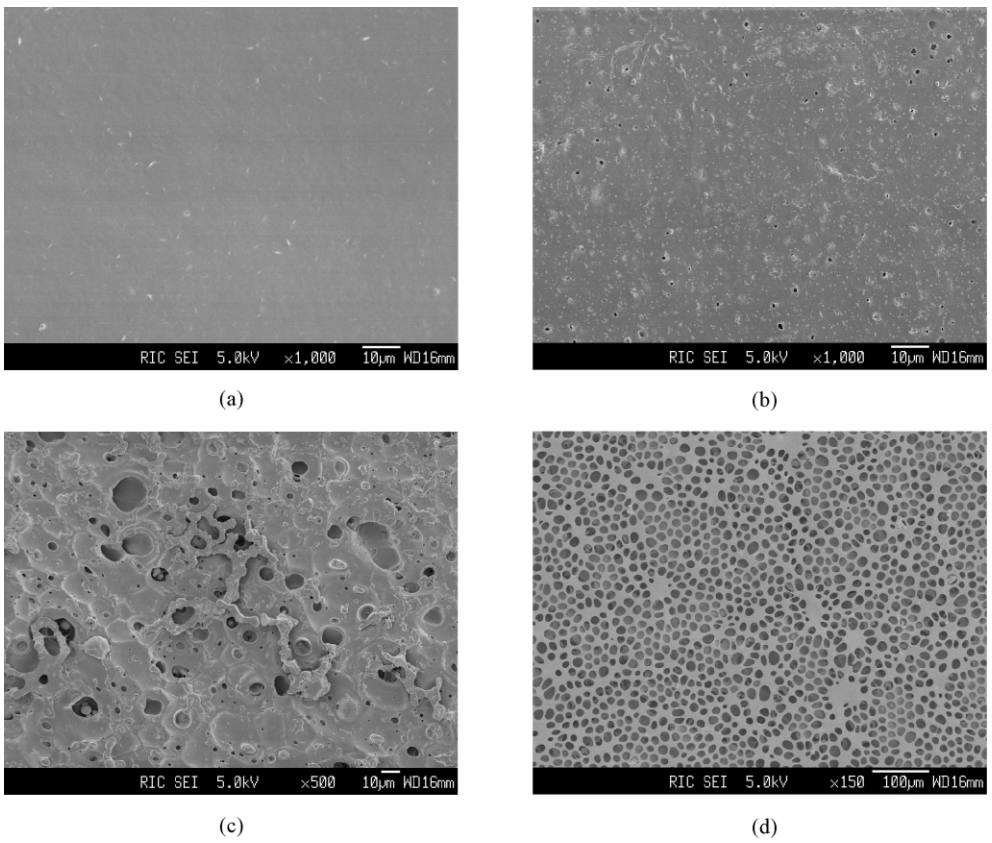

Fig. 14. SEM photographs of (a) PLA/PVAc 70/30, (b) PLA/P(VAc-*co*-VA)10 70/30, (c) PLA/P(VAc-*co*-VA)20 70/30, (d) PLA/P(VAc-*co*-VA)30 70/30.

were investigated by means of differential scanning calorimetry, synchrotron SAXS techniques, polarized optical microscopy and scanning electromagnetic microscopy.

PLA/PVAc blends were miscible systems for the entire composition regions, but for the blends with even 10% hydrolyzed PVAc copolymer the phase separation and double glass transition were observed.

With increasing neat PVAc content, the heat of fusion decreased and the melting peaks shifted to lower temperature in PLA/PVAc blends. The interaction parameters exhibited negative values for up to 10% hydrolyzed PVAc copolymer, but the values increased to positive ones with increasing the degree of hydrolysis. SAXS analysis and polarized optical microscopy observation indicated that a considerable amount of PVAc components located in the interlamellar region. But P(VAc-*co*-VA) component was expelled out of the interfibrillar regions of the PLA spherulites in PLA/P(VAc-*co*-VA) blends.

SEM analysis revealed that the significant phase separation occurred at the high degree of hydrolysis. In the case of PLA/P(VAc-*co*-VA)30 blend with 70/30 composition, the P(VAc-*co*-VA)30 copolymer formed the regular domains with a size of about 10 μm.

Acknowledgements

This work was supported by the Brain Korea 21 Project and the Basic Research program of the Korea Science and Engineering Foundation (grant No.1999-2-301-006-5). Experiments at Pohang Accelerator laboratory (PAL) were supported in part by the Ministry of Science and Technology (MOST) and Pohang Iron and Steel Co. (POSCO).

References

[1] Tsuji H, Ikada Y. Polymer 1996;37:595.
[2] Perego G, Domenico F, Bastioli C. J Appl Polym Sci 1996;59:37.
[3] Nijienhuis AJ, Colstee E, Grijpma DW, Pennings AJ. Polymer 1996; 37:5849.
[4] Gajria AM, Dave V, Gross RA, McCarthy SP. Polymer 1996;37:437.
[5] Sheth M, Kumar RA, Dave V, Gross RA, McCarthy SP. J Appl Polym Sci 1997;66:1495.
[6] Kricheldorf HR, Kreiser I. J Macromol Sci, Chem 1987;A24(11): 1345.
[7] Park JW, Im SS, Kim SH, Kim YH. Polym Engng Sci 2000;40(12): 2539.
[8] Park JW, Im SS. J Appl Polym Sci 2002;86:647.
[9] Tsuji H, Muramatsu H. Polym Degrad Stab 2001;71:403.
[10] Parada LG, Cesteros LC, Meaurio E, Katime I. Polymer 1998;39: 1019.

[11] Isasi JR, Cesteros LC, Katime I. Polymer 1995;36:1235.
[12] Xing P, Ai X, Dong L, Feng Z. Macromolecules 1998;31:6898.
[13] Defieuw G, Groeninckx G, Reynaers H. Polym Commun 1989;30: 267.
[14] Defieuw G, Groeninckx G, Reynaers H. Polymer 1989;30:595.
[15] Sauer BB, Hsiao BS. J Polym Sci, Part B: Polym Phys 1993;31:901.
[16] Hudson SD, Davis DD, Lovinger AJ. Macromolecules 1992;25:1759.
[17] Huo PP, Cebe P, Capel M. Macromolecules 1993;26:4275.
[18] Russell TP, Ito H, Wignall GD. Macromolecules 1988;21:1703.
[19] Bolze J, Kim J, Huang J-Y, Rah S, Youn HS, Lee B, Shin TJ, Ree M. Macromol Res 2002;10:2.
[20] Moritani T, Fujiwara Y. Macromolecules 1977;10:532.
[21] Toppet S, Lemstra PJ, Van der Velden G. Polymer 1983;24:507.
[22] Bugada DC, Rudin A. Polymer 1984;25:1759.
[23] Ito K, Yamashita Y. J Polym Sci 1965;A3:2165.
[24] Fox TG. Bull Am Phys Soc 1956;1:123.
[25] Gordon M, Taylor JS. J Appl Chem 1952;2:493.
[26] Gedde UW. Polymer physics. London: Chapman & Hall; 1995. p. 171.
[27] Hoffman JD, Weeks JJ. J Res Natl Bur Stand A 1962;66:13.
[28] Nishi T, Wang TT. Macromolecules 1975;8:909.
[29] Tsuji H, Ikada Y. Polymer 1995;36:2709.
[30] Hoffman JD, Miller RL, Marand H, Roitman DB. Macromolecules 1992;25:2221.
[31] Strobl GR, Schneider MJ, Voight-Martin IG. J Polym Sci, Part B: Polym Phys 1989;18:1361.
[32] Baltá-Calleja FJ, Vonk CG. X-ray scattering of synthetic polymers. Amsterdam: Elsevier; 1989. Chapter 7, p. 257.
[33] Verma R, Marand H, Hsiao B. Macromolecules 1996;29:7767.
[34] Hsiao BS, Wang Z, Yeh F, Gao Y, Sheth KC. Polymer 1999;40:3515.
[35] Talibuddin S, Wu L, Runt J, Lin JS. Macromolecules 1996;29:7527.
[36] Liu LZ, Chu B, Penning JP, Manley RSJ. Macromolecules 1997;30: 4398.
[37] Chen HL, Wang SF, Lin TL. Macromolecules 1998;31:8924.
[38] Vasnthakumari R, Pennings AJ. Polymer 1983;24:175.
[39] Ohkoshi I, Abe H, Doi Y. Polymer 2000;41:5985.
[40] Xing P, Dong L, An Y, Feng Z, Avella M, Martuscelli E. Macromolecules 1997;30:2726.
[41] Chen HL, Li LJ, Lin TL. Macromolecules 1998;31:2255.